Photodiagnosis and Photodynamic Therapy 27 (2019) 367–374

Contents lists available at ScienceDirect

Photodiagnosis and Photodynamic Therapy

journal homepage: www.elsevier.com/locate/pdpdt

Vandetanib sensitizes head and neck squamous cell carcinoma to photodynamic therapy through modulation of EGFR-dependent DNA repair and the tumour microenvironment

Pek Lim Chu[a], Waseem A. Shihabuddeen[b], Kar Perng Low[c], Dennis J.J. Poon[b], Bhuvaneswari Ramaswamy[c], Zhong-Guo Liang[b,d], Wen Long Nei[b], Kevin L.M. Chua[a,b], Patricia S.P. Thong[c], Khee Chee Soo[c], Eugenia L.L. Yeo[c], Melvin L.K. Chua[a,b,c,*]

[a] Oncology Academic Program, Duke-NUS Medical School, 169857, Singapore
[b] Division of Radiation Oncology, National Cancer Centre Singapore, 169610, Singapore
[c] Division of Medical Sciences, National Cancer Centre Singapore, 169610, Singapore
[d] Graduate School of Guangxi Medical University, Nanning, Guangxi, China

ARTICLE INFO

Keywords:
Photodynamic therapy
Vandetanib
Epidermal growth factor receptor
Head and neck cancer
Squamous cell carcinoma
DNA repair
Tumour microenvironment

ABSTRACT

Background: Epidermal growth factor receptor (EGFR) overexpression is characteristic in head and neck cancers and is associated with tumour regrowth following photodynamic therapy (PDT).
Purpose: We investigated vandetanib, which selectively blocks EGFR and vascular endothelial growth factor receptor-2 (VEGFR-2), to enhance the efficacy of PDT.
Methods: We assessed the *in vitro* therapeutic efficacy of: 1) vandetanib; 2) PDT with the photosensitizer Chlorin e6 (Fotolon®); and 3) combined PDT + vadetanib treatment in CAL-27 oral squamous cell carcinoma (OSCC) cell line by cell viability, γH2AX foci immunostaining, cell cycle arrest and western blot. We also performed *in vivo* tumour regression study and immunohistochemical staining of formalin-fixed paraffin-embedded (FFPE) regressed and regrown tumour tissues.
Results: First, we observed significantly higher cytotoxicity and residual DNA damage in vandetanib + PDT-treated CAL-27 OSCC cells than tumour cells treated with PDT alone. This is due to impaired DNA DSB repair caused by downregulation of EGFR-mediated DNA-dependent protein kinase catalytic subunit (DNA-PKcs) activation. Next, combined vandetanib and PDT resulted in significant tumour growth delay *in vivo* that is linked to reduction of PDT-induced EGFR phosphorylation and cellular proliferation, along with loss of tumour vasculature. In particular, we observed significant revascularisation of the microenvironment that is associated with upregulated ERK1/2 phosphorylation in regrown tumours post-vandetanib + PDT, thereby corroborating the importance of microenvironmental modification for the observed drug-PDT synergistic interaction.
Conclusion: Taken together, our data suggests that vandetanib enhances the efficacy of PDT through both direct and indirect effects on the cellular DNA repair machinery and tumour microenvironment, respectively.

1. Introduction

Oral cavity squamous cell carcinoma (OSCC) accounts for the main histologic subtype of neoplasms in the oral cavity, and these tumours are often linked to chronic carcinogenic insults like smoking, alcohol consumption, and betel nut chewing [1]. Surgery is the primary treatment modality for OSCC, and adjuvant chemo-radiotherapy is recommended for patients harbouring high-risk pathological features [2]. Nonetheless, despite these intensive treatment strategies, a substantial proportion (20–40%) of the patients still present with local recurrence, and in these individuals, therapeutic options are limited. Photodynamic therapy (PDT) represents a potential treatment modality for locally recurrent OSCC. It involves the systemic delivery of drugs known as photosensitisers, which tend to preferentially accumulate in

* Corresponding author at: Division of Radiation Oncology, National Cancer Centre Singapore, 11 Hospital Drive, 169610, Singapore.
E-mail addresses: jerry.chu@duke-nus.edu.sg (P.L. Chu), waseem.wshi@gmail.com (W.A. Shihabuddeen), low.kar.perng@nccs.com.sg (K.P. Low), dennis.poon.j.j@nccs.com.sg (D.J.J. Poon), bhuvsram@gmail.com (B. Ramaswamy), liangzhongguo@gxmu.edu.cn (Z.-G. Liang), kevin.chua.l.m@singhealth.com.sg (K.L.M. Chua), nmstsp@nccs.com.sg (P.S.P. Thong), soo.khee.chee@singhealth.com.sg (K.C. Soo), eugenia.yeo.l.l@nccs.com.sg (E.L.L. Yeo), Melvin.chua.l.k@singhealth.com.sg (M.L.K. Chua).

https://doi.org/10.1016/j.pdpdt.2019.06.008
Received 8 March 2019; Received in revised form 7 May 2019; Accepted 14 June 2019
Available online 09 July 2019

cancer cells than normal cells, but are only activated by light exposure to the region of interest [3–5]. Chlorin e6 (Ce6) is a highly effective second-generation photosensitiser in the production of more reactive oxygen species (ROS) and better skin tolerance as compared to porphyrin photosensitizers, such as 5-aminolevulinic acid (5-ALA) and porfimer sodium (Photofrin) [6,7]. In addition, Ce6 trisodium salt is a highly water soluble photosensitiser and can potentially achieve therapeutic active depth of up to 1.8 cm at the excitation wavelength of 665 nm [8], as a curative treatment for thicker tumour lesions. The activated photosensitisers then go on to form reactive oxygen species, which will induce tumour cell killing and vascular shutdown [5,9]. Consistent with these experimental observations, preliminary clinical evidence from early phase I/II trials on PDT in non-resectable head and neck cancers have indicated very optimistic response rates of 80% with PDT [9].

However, tumour recurrence and accelerated tumour repopulation eventually occur despite the initial response to PDT. These have been attributed to the activation of angiogenic pathways and epidermal growth factor receptor (EGFR) proliferative signalling [10,11]. Significant oxygen depletion following PDT causes tissue hypoxia and stimulation of angiogenic [12] and growth factor receptors [13]. Recent studies have further identified a novel radioprotective function of EGFR, which involves the radiation-induced nuclear translocation of the receptor and its interactions with the DNA-dependent protein kinase catalytic subunit (DNA-PKcs), a key component of the non-homologous end-joining (NHEJ) DNA repair pathway. Moreover, EGFR amplification is a common oncogenic driver event that is characteristic of head and neck squamous cell cancers (HNSCC) [14,15]. As shown by Ang et al. and several others [16], overexpression of EGFR is common in HNSCC, and importantly, predicted for inferior locoregional tumour control following primary radiotherapy. Targeting of the EGFR receptor therefore represents an appealing strategy to enhance the efficacy of PDT [17].

Here, we report for the first time the combination treatment of PDT and a multi-target tyrosine kinase inhibitor (TKI), vandetanib, which is a small (TKI) that selectively targets both EGFR and VEGFR-2 [18,19]. Our results demonstrated that vandetanib was able to significantly enhance the therapeutic efficacy of PDT in a synergistic manner both *in vitro* and *in vivo* using only a low dose of vandetanib (0.5 μM *in vitro* and 12.5 mg/kg *in vivo*). Further investigations into the mechanistic pathways revealed that this synergistic interaction is contributed by the additive effects of inhibition of EGFR oncogenic signalling, impairment of DNA double-strand break (DSB) NHEJ through inhibition of EGFR-dependent DNA-PKcs activation, and the vascular normalisation effect of vandetanib on the tumour microenvironment.

2. Materials and methods

2.1. Cell culture

Human OSCC cell line, CAL-27 (ATCC® CRL-2095™) was cultured in RPMI-1640 medium supplemented with 10% fetal bovine serum (FBS) (Gibco, USA), 1% each of non-essential amino acids (Gibco, USA), L-glutamine (Gibco, USA), sodium pyruvate (Gibco, USA) and 100 units/mL penicillin/streptomycin (Gibco, USA). Cells were incubated at 37 °C in a 5% CO_2 and 95% humidified incubator.

2.2. Chemicals and reagents

The photosensitiser Fotolon® was provided by APOCARE Pharma GmBH, Germany. Vandetanib was purchased from Selleckchem (Houston, TX, USA) and stored at -20 °C. Vandetanib was dissolved in dimethyl sulfoxide (DMSO) and used for *in vitro* assays.

2.3. Cytotoxicity assay

5×10^3 CAL-27 cells/well were seeded into 96-well plates. After 18 h of incubation, cells were rinsed with 1X phosphate buffered saline (PBS) and incubated with different concentration of Ce6 (0.5 μM, 1 μM, 2 μM, 5 μM and 10 μM) prepared in serum-free RPMI for PDT treatment; and serum-free RPMI for control and vandetanib (ZD) groups, for 3 h. After 3 h, all the wells were rinsed with 1X PBS and incubated with 2% FBS-RPMI medium. For vandetanib treatment, the cells were incubated with different concentrations of vandetanib (0.5 μM, 1 μM, 2 μM, 4 μM, 6 μM, 8 μM and 10 μM). Negative controls (cells only) and vehicle control (0.1% DMSO) were included. For the plates undergoing PDT treatment, the cells were irradiated at 665 nm with light doses of 0.5 J/cm^2 or 1.0 J/cm^2. For combination treatment, 0.5 μM Ce6 and 0.5 J/cm^2 light dose were used for PDT together with 0.5 μM or 1 μM vandetanib. After 72 h incubation, cell viability was measured using CellTiter-Glo® Luminescent Cell Viability Assay kit (Promega, USA). Luminescent signals were measured by a Tecan Safire2™ microplate reader. The results were expressed as a percentage of the control, which was defined as 100%. The dose-effect curve of vandetanib was analysed using GraphPad Prism version 5.0 (San Diego, California, USA) and the half maximal inhibitory concentration (IC_{50}) was determined.

2.4. γH2AX foci immunostaining

CAL-27 cells were seeded on glass coverslips in 6-well plate. The cells were incubated for 18 h at 37 °C with 5% CO_2. Then, the cells were treated with vandetanib (0.5 μM), PDT (0.5 μM Ce6, 0.5 J/cm^2) or combination of both. At different time points following PDT treatment (0 h, 1 h, 4 h, 8 h, 24 h and 24 h post-removal of vandetanib), cells were rinsed with PBS and fixed with 4% paraformaldehyde. The cells were washed with PBS and blocked with 5% FBS in PBS at room temperature for 1 h. Cells were then incubated with the primary antibody anti-γ-H2AX mouse monoclonal antibody (1:5000 dilution in PBS with 1% FBS and 0.3% Triton X-100; Merck, MA), overnight at 4 °C. After PBS wash, cells were incubated with Alexa Fluor 488 secondary antibodies (1:1500 dilution in PBS with 1% FBS and 0.3% Triton X-100; Molecular probe, Life Technologies, CA) for 1 h in the dark. Cells were washed again and counterstained with Hoechst 33342 (1:5000 dilution in PBS; Life Technologies, CA) for 15 min. Finally, cells were washed with PBS and mounted onto glass slides using Prolong® Gold Antifade Reagent (Molecular probe, Life Technologies, CA).

Slides were scanned with the NIS Elements software on a confocal laser microscope- Nikon N-STORM (Nikon Instruments Inc., New York). Bitplane Imaris software v8.2 was used to stack the multiplane images (minimum of 10 planes per sample), and to process the Z-stacked images for foci scoring using a uniform threshold parameter (0.6 μm cut-off for foci diameter). All treated and control samples were performed in duplicates, with a minimum of 50 cells scored per sample.

2.5. Cell cycle analysis

CAL-27 cells were seeded in 6-well plate and treated as described in the previous section. After 24 h of incubation, the cells were washed twice with ice cold PBS and harvested. The cell pellets were re-suspended with 500 μl of PBS each and added into 70% ice cold ethanol. The cells were kept in -20 °C overnight. Then, the cells were washed twice with 5 ml of ice-cold PBS and stained with FxCycle™ PI/RNase Staining Solution (Molecular Probes, Life Technologies, CA) and incubated at room temperature for 15 min. The percentage of the cell population in each phase of cell cycle was measured using BD FACSCanto™ II flow cytometer (USA) and the data was analysed using FlowJo software (version 7.6.1).

2.6. Western blot analysis

For EGFR signalling study, 2×10^5 cells/well were seeded in complete medium in 6-well plates and incubated at 37 °C in 5% CO_2 incubator for 18 h. The cells were starved for 24 h in serum-free culture medium and were then treated with vandetanib for 90 min followed by EGF (50 ng/ml) stimulation for 15 min. Total cell lysates were obtained by using Pierce RIPA buffer (Life Technologies, CA) with 1X Protease/Phosphatase Inhibitor Cocktail (Cell Signaling Technology, USA) and stored at −80 °C until use.

For the DNA repair study, 4.2×10^6 cells were seeded in a T-75 culture flask. Treatment settings used were the same as in the DNA damage response assay. Nuclear proteins were obtained using Cell Fractionation kit (Cell Signaling Technology, MA, USA), according to manufacturer's protocol. Briefly, the cells were harvested and washed with cold PBS. The cell pellet was first resuspended in CIB buffer and spun at 500 ×g for 5 min to collect the cytoplasmic fraction. Then the pellet was resuspended in MIB buffer and spun at 8000 ×g for 5 min to collect the membrane and organelle fraction. Finally, the pellet was lysed in RIPA buffer and collected as nuclear fraction. All fractions were stored at −80 °C until use.

Equal amount of proteins was resolved in a 10% sodium dodecyl sulfate-polyacrylamide (SDS-PAGE) gel and immunoblotted against phospho-EGFR, EGFR, phospho-STAT3, STAT3, phospho-Akt, Akt, phospho-p44/42 MAPK, p44/42 MAPK, phospho-ATM, ATM, phospho-histone H2AX (Merck, MA), DNA-PKcs, phospho-DNA-PKcs (Thr2609) (Abcam, MA, USA), phospho-Ku70 (Abcam), Ku70, Ku80, Rad51 (Life Technologies), p84 (GeneTex, CA), GAPDH. Quantification of binding was measured using horseradish peroxidase (HRP)-conjugated secondary antibodies and ECL system (Amersham Hyperfilm ECL, GE Healthcare, USA). All primary antibodies and secondary antibodies were obtained from Cell Signaling Technology (MA, USA) unless stated otherwise (See Supplementary Appendix).

2.7. CAL-27 xenograft tumour regression

All procedures performed were approved by the Institutional Animal Care and Use Committee (IACUC, 2015/SHS/1071) Singapore Health Services Pte Ltd. A suspension of 5×10^6 CAL-27 cells in 100 µl of Matrigel was injected subcutaneously into the flank of NCr nude mice of 6–8 weeks old (Invivos, Singapore). When the tumours reached 200 mm^3, the mice were randomised into four groups. Vandetanib was dissolved in PBS with 1% Tween 80. Mice were orally treated with vehicle control, 12.5 mg/kg vandetanib once daily for 14 days, PDT alone or combination of PDT and vandetanib. For PDT treatment, the mice were injected intravenously with 10 mg/kg of Ce6, followed by an irradiation at 665 nm using a laser light source (LVI Technology Inc, South Korea) 3 h post-injection. A light dose of 150 J/cm^2 at a fluence rate of 100 mW/cm^2 was delivered to the tumours. The tumour volume ($\pi/6 \times d1 \times d2 \times d3$) was determined every other day, where d1, d2 and d3 are the tumour dimensions in three orthogonal directions. The mice were euthanised when the tumour size reached the ethical limit of 2 cm^3. For mechanistic study of treatments, the tumours were harvested on day 8 – when the tumours of PDT treated xenografts have regrown while combination treated xenografts were still regressing. Each treatment group had a minimum of n = 3. Tumour tissues harvested and evaluated by haematoxylin and eosin and immunohistochemistry.

2.8. Immunohistochemical analysis

The paraffin-embedded sections of 5 µm thickness were deparaffinised in Neo-clear (Merck, MA), rehydrated in ethanol series and antigen retrieval by heating in citric acid buffer at 95 °C for 30 min. Tissue sections were cooled and immersed in 3% hydrogen peroxide (Sigma, US) for 10 min. Then, the tissue sections were washed twice with distilled water and once with Tris-buffered saline with 0.1% Tween 20 (TBST) buffer and blocked with 5% goat serum at room temperature for one hour. Tissues were incubated with primary antibodies (See Supplementary Appendix) against CD31, Ki67, phospho-EGFR, phospho-ERK1/2 for overnight at 4 °C. After three washes with TBST, tissues were incubated with REAL™ EnVision™/HRP-labeled goat anti-rabbit/mouse secondary antibody (Dako, Glostrup, Denmark) for one hour at room temperature. Brown colour was detected at target antigen site by adding diaminobenzidine (DAB+) chromogen and counter stained with haematoxylin for the nuclei. Lastly, tissues were dehydrated and mounted. Quantification analysis of IHC images were performed using Fiji [20]. The microvessel density (MVD) was quantified by measuring the number of microvessel within a defined area x 100%.

2.9. Statistical analysis

Comparisons between groups for cell cytotoxicity, mean γH2AX foci number and tumour volume were tested using one-way analysis of variance (ANOVA) with Bonferroni correction for multiple comparisons. Student *t*-test was used for IHC of Ki67, (MVD, phospho-EGFR and phospho-ERK1/2. All statistical analyses were performed using GraphPad Prism (version 5.0, San Diego, California, USA) software. A P value < 0.05 was considered statistically significant.

3. Results

3.1. Vandetanib enhanced cytotoxicity of PDT in CAL-27 cells

Individually, vandetanib and PDT exhibited cytotoxicity on CAL-27 cells in dose-dependent manners (Fig. 1A and B). The IC50 of vandetanib on CAL-27 cells was determined at 1.2 µM. For PDT, 1.0 J/cm^2 of light dose resulted in high levels of cytotoxicity on CAL-27 cells, even at low concentrations of Ce6. The IC50 value for PDT with 0.5 J/cm^2 was determined at 1.06 µM of Ce6. We therefore determined the suboptimal PDT condition for *in vitro* assays to be 0.5 µM Ce6 with a light dose of 0.5 J/cm^2. Next, we tested if the combination of vandetanib and PDT resulted in increased cell killing over either treatment alone. We observed a synergistic effect of drug with PDT when PDT-exposed cells were treated with 0.5 µM and 1.0 µM of vandetanib; PDT treatment alone resulted in 81.0% ± 7.5% of cell viability, while cell viability of drug-treated cells were 54.6 ± 2.8% (0.5 µM) and 47.6 ± 0.9% (1.0 µM; Fig. 1C; $P < 0.001$).

3.2. Vandetanib sensitises CAL-27 cells to PDT-induced DNA damage

Next, we tested if impaired DSB repair was a mechanism underpinning the increased cytotoxicity of CAL-27 with combination vandetanib and PDT. In the vandetanib alone- and PDT-treated cells, we observed an initial increase of γH2AX foci at 4 h post-drug exposure that is followed by stabilisation of foci counts at the subsequent timepoints (Fig. 2A). This contrasts to the vandetanib + PDT-treated cells, whereby we observed increasing accumulation of foci over 24 h, which remained elevated even 24 h following removal of the drug ($P < 0.001$). This is consistent with western blot analyses showing increased γH2AX expression (Fig. 2B), and G1 checkpoint arrest that corresponds to high levels of DSB at 24 h post-vandetanib + PDT (Fig. 2C).

3.3. Vandetanib inhibits PDT-induced nuclear accumulation of EGFR and impaired DNA-PKcs-dependent NHEJ repair

We further investigated the nature of DSB repair impairment with combination therapy. We first show that upon EGF ligand stimulation, vandetanib reduced the phosphorylation of EGFR and the downstream targets of protein kinase B (Akt), signal transducer and activator of transcription 3 (STAT3) and mitogen activated protein kinase (MAPK)

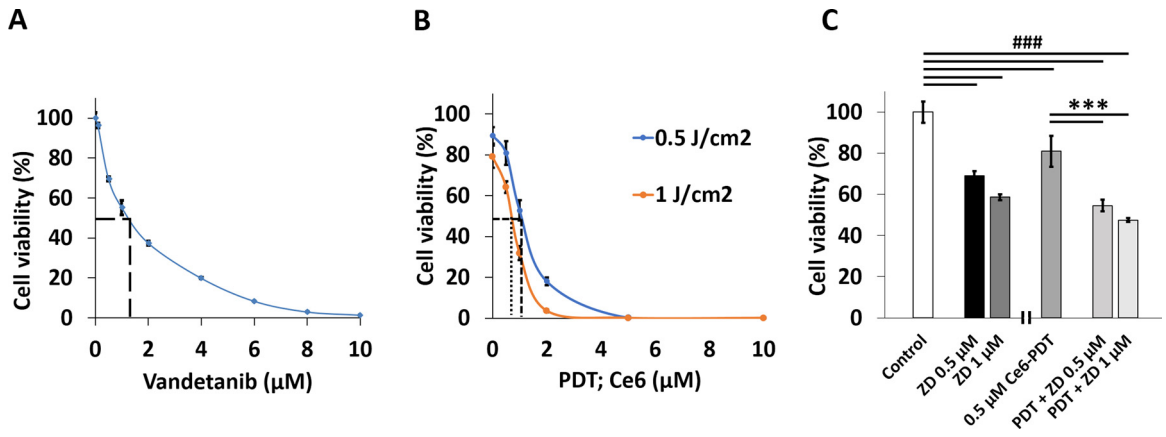

Fig. 1. Vandetanib enhanced cytotoxicity of PDT in CAL-27 cells.
(A) Cells were treated with vandetanib for 72 h and IC_{50} was determined. (B) Cells were treated with different concentrations of Ce6 and irradiated at 665 nm with light doses of 0.5 J/cm^2 or 1.0 J/cm^2, and further incubated for 72 h. (C) Cells were treated with PDT and with/without vandetanib (ZD), incubated for 72 h. The significant difference of cell viability between each group was analysed using the one-way ANOVA; $^{###}P < 0.001$ *vs* control, $^{***}P < 0.001$ *vs* PDT. Combination treatment (PDT + ZD) were significantly more cytotoxic than ZD alone treatment ($P < 0.001$) and PDT alone treatment ($P < 0.001$). Cell viability percentage was obtained by normalising against control/drug solvent control. The percentage of cell viability was expressed as mean ± SD.

in a dose-dependent manner (Fig. 3A). PDT treatment resulted in nuclear accumulation of EGFR and increased expression of phospho-DNA-PKcs, but not phospho-ATM (Fig. 3B). In contrast, we observed a reduced nuclear import of EGFR and phosphorylation of DNA-PKcs protein in the combined treatment panel. This however did not result in a downstream effect on Ku70/Ku80 proteins. Additionally, we did not

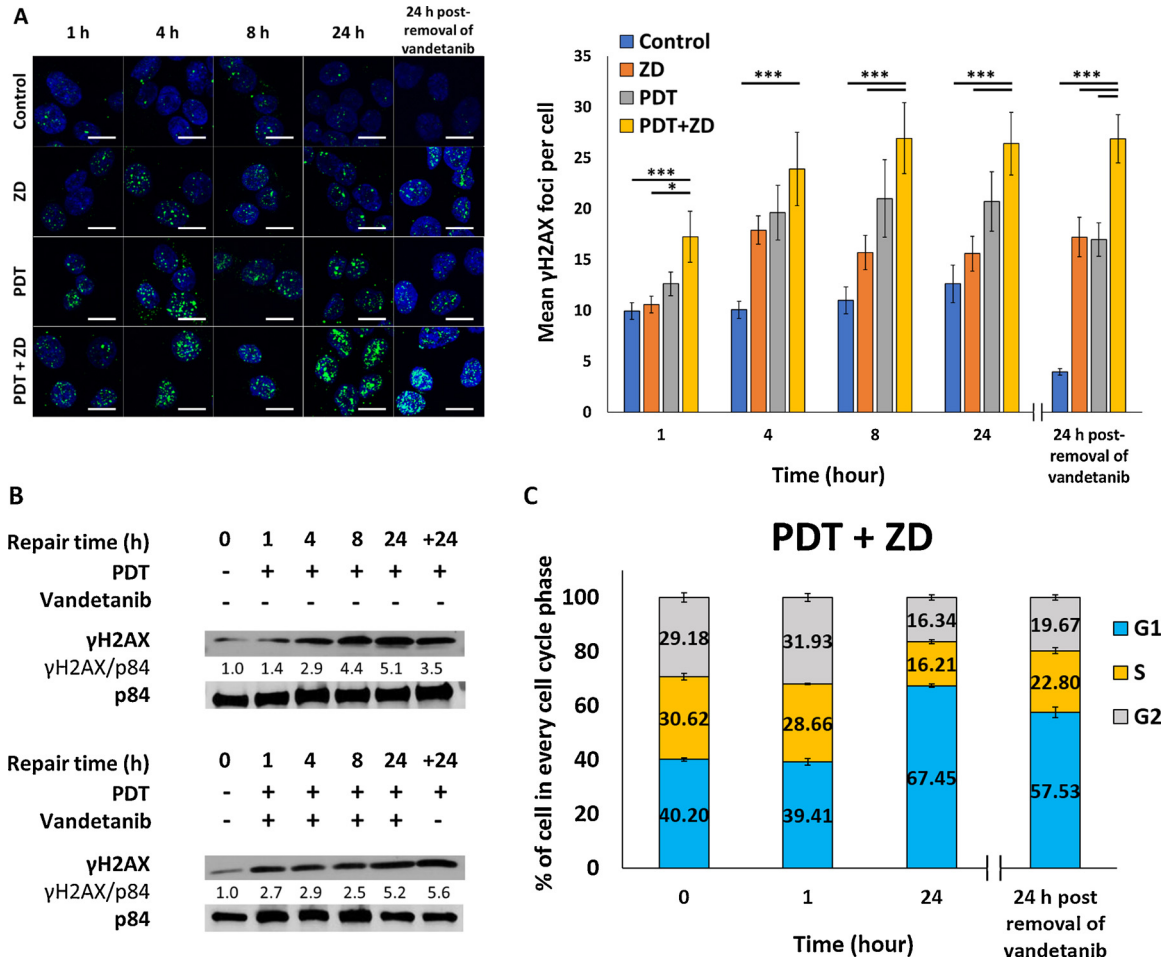

Fig. 2. Vandetanib increases PDT-mediated cytotoxicity via impairment of DNA DSB repair.
(A) γH2AX foci quantification at various time-points following PDT (1, 4, 8, 24 and 24-h post removal of vandetanib). Image magnification is 200X, scale bar represents 100 μM. (B) Western blot confirming increased residual damage at 24 h post-removal of drug. (C) Cell cycle alteration in response to the DNA damage resulted by combination treatment. The percentage of each phase of cell cycle were presented as means ± SD.

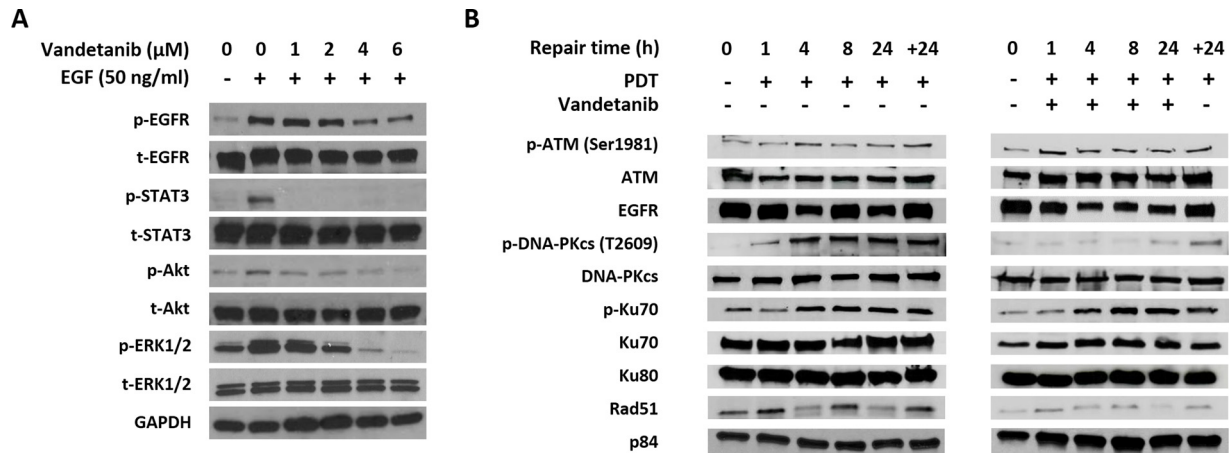

Fig. 3. Vandetanib impaired DNA-PKcs-dependent NHEJ repair through EGFR inhibition.
(A) Western blot of vandetanib on EGFR signalling inhibition. Serum-starved CAL-27 cells were treated with/without vandetanib at different concentrations for 90 min, followed by EGF (50 ng/mL) stimulation. (B) Western blot of DNA repair proteins confirming the impairment of NHEJ repair through DNA-PKcs phosphorylation inhibition by vandetanib.

observe any compensatory increase in Rad51 protein expression, which would indicate a shift towards homologous recombination repair of DSB; this is however not unexpected, given the predominance of vandetanib + PDT-treated cells residing in the G1 phase of the cell cycle (Fig. 2C). The reduced DNA-PKcs expression corresponded to loss of total nuclear EGFR signals that is reversed upon removal of the vandetanib. Taken together, the data suggests that the potentiation of PDT lethality on CAL-27 cells by vandetanib *in vitro* is primarily due to inhibition of EGFR-mediated activation of DNA-PKcs-dependent NHEJ.

3.4. Vandetanib modulates the tumour microenvironment post-PDT treatment in vivo

The efficacies of PDT, vandetanib and combination treatment were evaluated in CAL-27 tumour xenografts (Fig. 4A). When PDT treatment was combined with low dose of vandetanib, we observed a significant tumour growth delay (Fig. 4B) starting on day-4 post-treatment as compared to the PDT-alone treatment arm (day 4, $P = 0.0058$; day 6, $P = 0.0435$; day 8, $P = 0.0308$; day 10, $P = 0.0274$; day 12, $P = 0.0207$; day 14, $P = 0.0254$). However, no appreciable tumour growth delay was observed in the vandetanib-alone treatment arm. These findings were consistent with the median survival of mice between the treatment arms (median survival of 20 d (vandetanib + PDT) *vs* 10 d (control); Fig. 4C). Interestingly, we observed a distinct morphological appearance of necrotic tumour cores in the regrown tumours post-combination treatment (Fig. 4D), showing that the tumour core was effectively targeted by PDT and the regrowth likely started from the tumour periphery.

We next harvested tumours from the xenografts at two time-points: an early time-point (8 d post-treatment) to determine the mechanisms underpinning the synergistic efficacy; and a late time-point when tumours regrow to a pre-specified size to investigate the potential mechanisms of tumour regrowth (Fig. 4A). At 8 d, we observed that both vehicle- and vandetanib-treated tumours continued to proliferate as evidenced by the high Ki67 expression and few apoptotic cells (Fig. 5A and C). Although we did not obtain an appreciable tumour growth delay with vandetanib treatment, the MVD was reduced as compared to control ($P < 0.001$; Fig. 5A and B). Likewise, we observed significant tumour cell killing and overgrowth of stromal cells that correspond to low Ki67 expression and MVD after PDT treatment (Fig. 5A-C). Interestingly, we observed a high expression of phospho-EGFR post-PDT (Fig. 5D), which is likely a compensatory response to treatment. Combination vandetanib-PDT-treated tumours demonstrated reduced phospho-EGFR expression compared to PDT-alone ($P < 0.0001$), which coupled with low Ki67 expression ($P < 0.0001$) and MVD ($P = 0.0001$), corresponded to the most pronounced tumour growth delay *in vivo*.

Interestingly, we made a few key observations in the later time-point regrown tumours. Foremost, we observed significant revascularisation of the microenvironment ($P < 0.0001$ *vs* early time-point tumours) and high expression of Ki67 in these tumours (Fig. 5A-C). In addition, phosphorylation of extracellular signal-regulated kinase-1 and kinase-2 (ERK1/2) was not observed in the post-PDT-treated regrown tumours (Fig. 5A and E), but interestingly it was significantly upregulated in the regrown tumours post-vandetanib + PDT ($P < 0.0001$). This would suggest that MAPK-ERK1/2 signalling axis is a specific mechanism driving tumour regrowth following the combination of vandetanib and PDT. Taken together, our findings present a model (Fig. 5F) whereby the direct effects on the DNA repair machinery in these cells and the modulation on the tumour vasculature contribute to the synergistic interaction between vandetanib and PDT. However, targeting by vandetanib also results in the compensatory upregulation of phospho-ERK1/2 that appears to be exclusive to the combination with this drug.

4. Discussion

PDT-induced EGFR expression has been reported to be a main driver of tumour recurrence after PDT. This is particularly relevant in OSCC/HNSCC where overexpression of EGFR is commonly observed [17,18], and this intrinsic molecular phenotype only further predisposes these tumours to recur post-PDT. To exploit this tumour-specific characteristic, we investigated the efficacy of vandetanib, a multitarget kinase inhibitor, as a sensitiser of PDT-directed tumour targeting. Ce6-PDT mediated apoptosis has been reported as the prominent mode of cell death involving biochemical changes such as chromatin condensation, DNA fragmentation and others [21–23]. Here, we show that vandetanib impairs the DNA repair machinery through inhibition of PDT-induced nuclear trafficking of EGFR and as a result, affects the downstream EGFR-mediated activation of DNA-PKcs-dependent NHEJ; this is potentiated by the lack of a compensatory HR response due to the arrest of cells in G1 phase of the cell cycle. Taken together, vandetanib inhibited the repair of both cell proliferation-induced and PDT-induced apoptosis-mediated DNA damage, resulted in the accumulation of γH2AX foci and translated to a higher direct cytotoxicity. This, coupled with the tumour vasculature shutdown and normalisation effect by PDT and vandetanib, resulted in significant tumour growth delay *in vivo*. Nonetheless, treatment with vandetanib also led to a compensatory

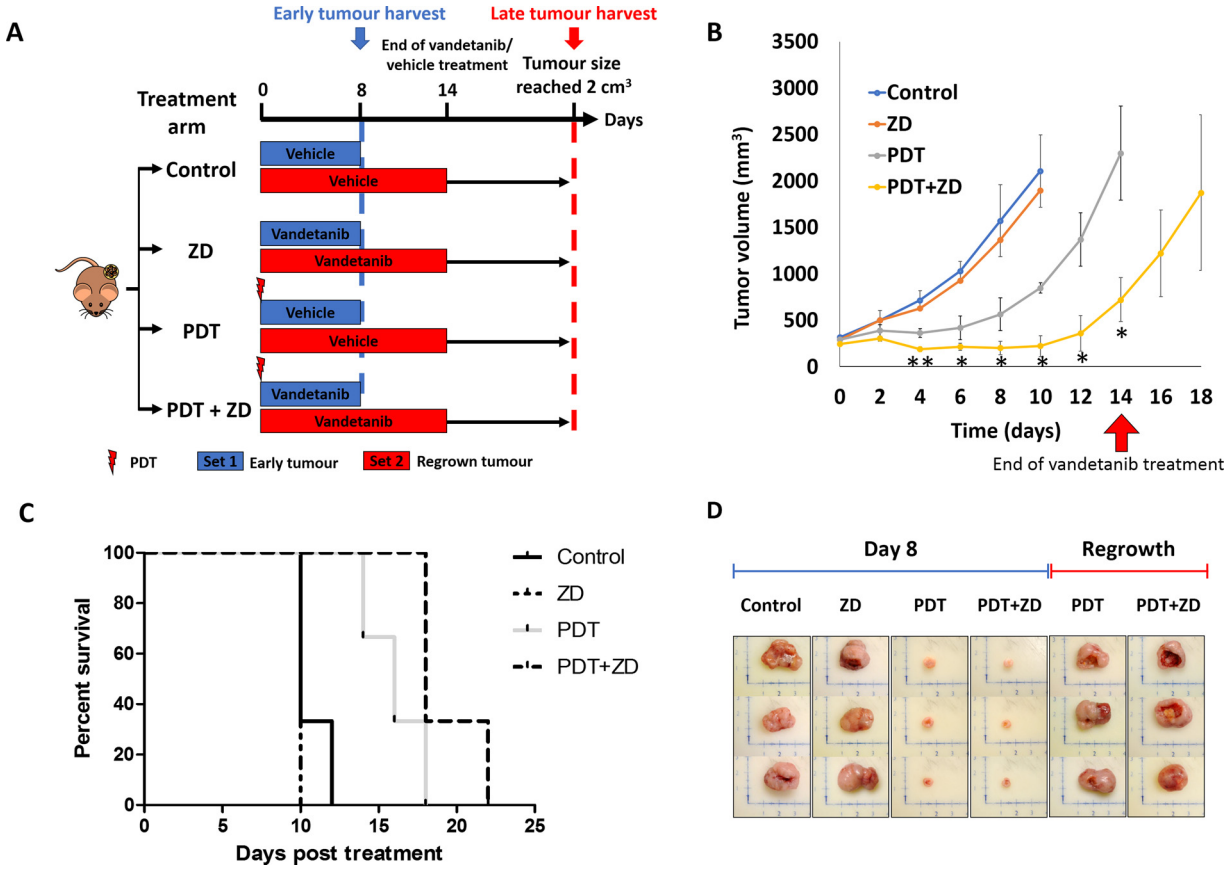

Fig. 4. Combination of PDT and vandetanib delays tumour growth and enhances the survival rate in CAL-27 xenografts.
(A, B) Tumour growth in response to vehicle, individual treatment of vandetanib (12.5 mg/kg daily), PDT (10 mg/kg Ce6, 150 J/cm^2) and combination of both. Each treatment group had a minimum of n = 3. Treatment of vehicle and vandetanib was administrated for 14 days. Treated and non-treated tumours were allowed to grow and reached the ethical limit of 2 cm^3. Tumours of animals in Set 1 were harvested early (8 d) for mechanistic studies, while those in Set 2 were harvested later to study end-point and regrown tumours. The tumour volume was expressed as mean ± SE of each group. PDT-mediated tumour growth delay was further enhanced by vandetanib. The difference in tumour growth between PDT-alone treatment arm and combination treatment arm was analysed using the Student's *t*-test; *P < 0.05, **P < 0.01. (C) Kaplan-Meier survival curve was plotted as the time points of euthanisation, when the tumour size reached 2 cm^3. (D) Growing tumour tissues at 8 d and regrown tumours were harvested for mechanistic study.

activation of the MAPK-ERK1/2 signalling axis, and thus future combination therapy strategies ought to include novel ERK1/2 inhibitor compounds.

Constitutive PDT-mediated EGFR activation has been reported as a dominant tumour recurrence mechanism following PDT [11,13,24]. In our pre-clinical study, we observed a significant reduction in the PDT-induced EGFR phosphorylation, cellular proliferation and MVD in the 8 d tumour post-combination vandetanib + PDT compared to PDT-alone, suggesting that the drug exerts its synergism with PDT through direct (cellular) and indirect (microenvironmental) effects. This is consistent with past studies that have demonstrated that dual targeting of EGFR and VEGFR leads to increased apoptosis of tumour cells and reduce neovascularisation by tumour-associated endothelial cells [25,26].

The unique finding of our study relates to the restoration of proliferation and vascularisation, coupled with compensatory increase of ERK1/2 phosphorylation in the regrown tumours post-vandetanib + PDT. This contrasts our observations *in vitro* whereby we observed a reduced downstream activation of ERK1/2 with vandetanib treatment alone on CAL-27 cells (Fig. 3A), thereby implying that this *in vitro* effect is likely transient and not recapitulated *in vivo*. Interestingly, the compensatory ERK1/2 phosphorylation *in vivo* appears to be an exclusive post-vandetanib exposure effect, and may be supported by a previous study showing the activation of the MAPK pathway in G1 phase-arrested tumour cells [27]. A sustained activation of ERK/MAPK in OSCC [28] and oral tongue squamous cell carcinoma (OTSCC) [29] patients has been reported and suggesting its pivotal role in cell proliferation and carcinogenesis. While further mechanistic work is beyond the scope of this current study, a thorough understanding regarding the mechanisms involved in tumour recurrence is crucial to improve the therapeutic ratio of this treatment strategy.

Our study is not without limitations. Certainly, given that this is an immune-deficient model, other mechanisms apart from direct cell killing and modulation of the tumour microenvironment could also potentiate the efficacy between vandetanib + PDT. For example, in our model, we showed that vandetanib modulates the tumour microenvironment, and given the influence of the microenvironment on the immune response, other mechanisms could be observed if the experiments were conducted in an immune-competent model. Next, while we showcased a compensatory expression of phospho-ERK1/2 in the regrown tumours following PDT + vandetanib, we did not investigate for mechanisms underpinning this phenomenon.

Here, we presented a model confirming the direct and off-target effects of a small molecule multi-target TKI when combined with PDT. However, we observed eventual tumour regrowth, which emphasises the need to develop novel agents for a multi-target combination therapy approach, so as to enhance the local control of HNSCC tumours.

Author contributions

Data acquisition: PC, WS, KL, DP, BR, ZL, WN, KC, PT, EY.
Statistical analyses: PC, BR, KC, EY and MC.
Study conception and design: PC, BR, PT, EY, KS and MC.

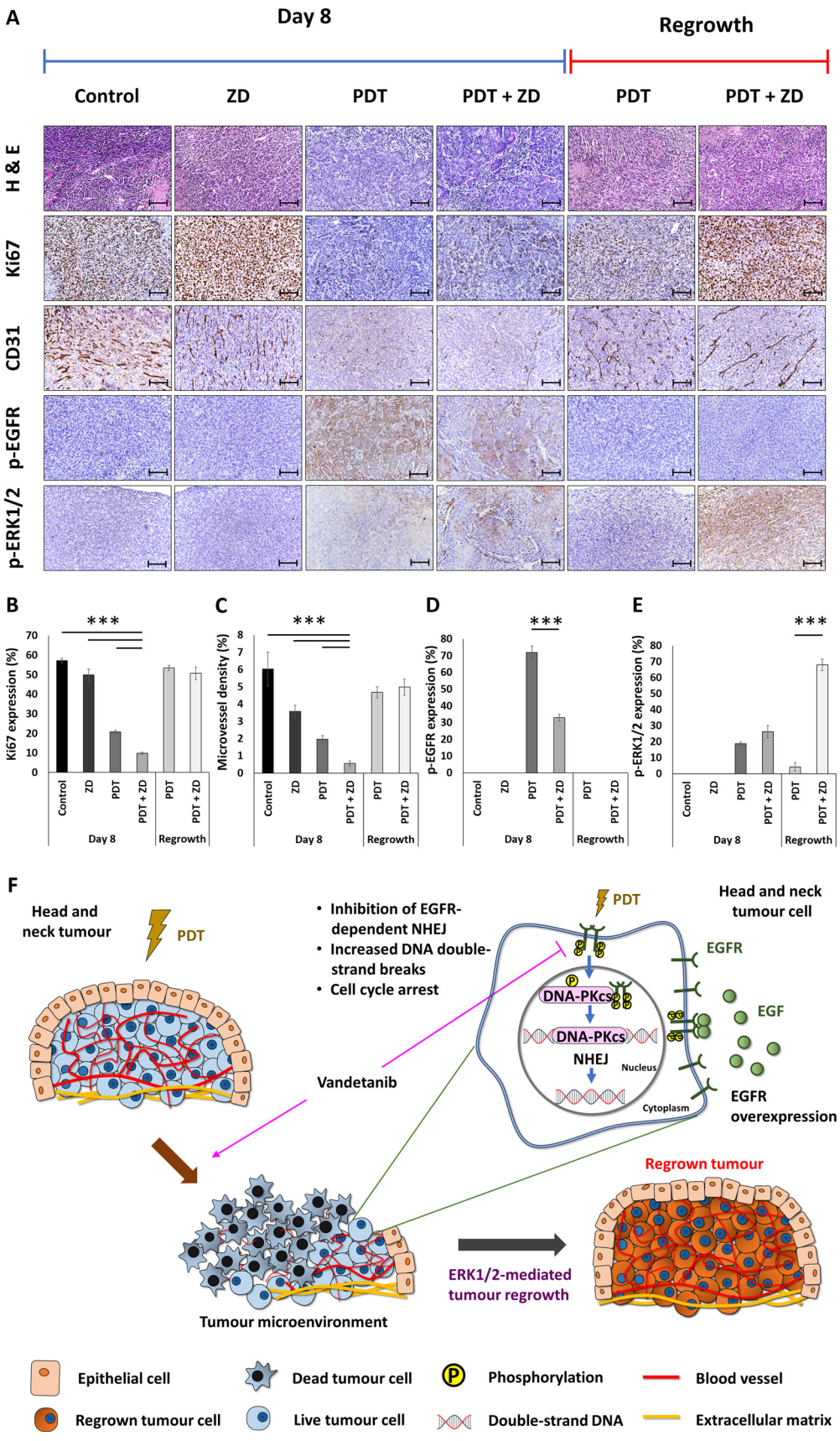

Fig. 5. Vandetanib modulates the tumour microenvironment of PDT-treated tumours attributable to inhibition of PDT-induced EGFR expression and vascular normalisation which is followed by tumour re-growth associated with up-regulated ERK1/2 phosphorylation.
(A) Hematoxylin and eosin staining and immunohistochemistry staining of CAL-27 xenograft tumours and quantification analysis for (B) Ki67 (C) CD31 (D) phospho-EGFR and (E) phospho-ERK1/2. Representative images are shown. Image magnification is 1000X, scale bar represents 100 μM. The difference in marker expression between groups was analysed using the Student's *t*-test; ***P < 0.0001. (F) Schematic illustration of enhanced PDT efficacy by vandetanib in HNSCC.

Study supervision: EY and MC.
Wrote the first draft of the manuscript: PC, EY and MC.
All authors approved the manuscript.

Financial disclosure

MC declares honorarium and advisory board for Janssen, Astellas, Varian, Ferring Singapore and Astra Zeneca. MC declares Structured research agreement/Research funding with Ferring Singapore, GenomeDx Biosciences, Varian and MedLever.

Acknowledgements

The authors thank all members of the Chua laboratory for support and guidance. This study was supported by a SingHealth Foundation, Singapore (SHF/FG573P/2014), Ministry of Education (MOE) Tier 3, Singapore (MOE2016-T3-1-004), National Medical Research Council: NMRC Clinician Scientist Award, Singapore (NMRC/CSA-INV/0027/2018) and National Research Foundation (NRF) Competitive Research Programme, Singapore (NRF-CRP17-2017-05).

Appendix A. Supplementary data

Supplementary material related to this article can be found, in the online version, at doi:https://doi.org/10.1016/j.pdpdt.2019.06.008.

References

[1] W.-J. Lin, R.-S. Jiang, S.-H. Wu, F.-J. Chen, S.-A. Liu, Smoking, alcohol, and betel quid and oral cancer: a prospective cohort study, J. Oncol. (2011) 525976, https://doi.org/10.1155/2011/525976.
[2] S.R. Quinlan-Davidson, A.S.R. Mohamed, J.N. Myers, G.B. Gunn, F.M. Johnson, H. Skinner, B.M. Beadle, A.M. Gillenwater, J. Phan, S.J. Frank, W.N. William, A.J. Wong, S.Y. Lai, C.D. Fuller, W.H. Morrison, D.I. Rosenthal, A.S. Garden, A.S. Garden, Outcomes of oral cavity cancer patients treated with surgery followed by postoperative intensity modulated radiation therapy, Oral Oncol. 72 (2017) 90–97, https://doi.org/10.1016/j.oraloncology.2017.07.002.
[3] B.C. Wilson, Photodynamic therapy for cancer: principles, Can. J. Gastroenterol. 16 (2002) 393–396 http://www.ncbi.nlm.nih.gov/pubmed/12096303.
[4] M.B. Vrouenraets, G.W.M. Visser, G.B. Snow, G.A.M.S. van Dongen, Basic principles, applications in oncology and improved selectivity of photodynamic therapy, Anticancer Res. 23 (1B) (2003) 505–522 http://www.ncbi.nlm.nih.gov/pubmed/12680139.
[5] D.E.J.G.J. Dolmans, D. Fukumura, R.K. Jain, Photodynamic therapy for cancer, Nat. Rev. Cancer 3 (2003) 380–387, https://doi.org/10.1038/nrc1071.
[6] A. Juzeniene, Chlorin e6-based photosensitizers for photodynamic therapy and photodiagnosis, Photodiagnosis Photodyn. Ther. 6 (2009) 94–96, https://doi.org/10.1016/j.pdpdt.2009.06.001.
[7] S. Kwiatkowski, B. Knap, D. Przystupski, J. Saczko, E. Kędzierska, K. Knap-Czop, J. Kotlińska, O. Michel, K. Kotowski, J. Kulbacka, Photodynamic therapy – mechanisms, photosensitizers and combinations, Biomed. Pharmacother. 106 (2018) 1098–1107, https://doi.org/10.1016/j.biopha.2018.07.049.
[8] D. Hüttenberger, H. Sudhoff, L. Freitag, M. Haupt, Systemic photodynamic therapy with Fotolon ® – A promising approach for tumor treatment – Not only for superficial lesions, Photodiagnosis Photodyn. Ther. 17 (2017) A69, https://doi.org/10.1016/j.pdpdt.2017.01.157.
[9] P. Agostinis, K. Berg, K.A. Cengel, T.H. Foster, A.W. Girotti, S.O. Gollnick, S.M. Hahn, M.R. Hamblin, A. Juzeniene, D. Kessel, M. Korbelik, J. Moan, P. Mroz, D. Nowis, J. Piette, B.C. Wilson, J. Golab, Photodynamic therapy of cancer: an update, CA Cancer J. Clin. 61 (2011) 250–281, https://doi.org/10.3322/caac.20114.
[10] S.M. Gallagher-Colombo, A.L. Maas, M. Yuan, T.M. Busch, Photodynamic therapy-induced angiogenic signaling: consequences and solutions to improve therapeutic response, Isr. J. Chem. 52 (2012) 681–690, https://doi.org/10.1002/ijch.201200011.
[11] C. Edmonds, S. Hagan, S.M. Gallagher-Colombo, T.M. Busch, K.A. Cengel, Photodynamic therapy activated signaling from epidermal growth factor receptor and STAT3, Cancer Biol. Ther. 13 (2012) 1463–1470, https://doi.org/10.4161/cbt.22256.
[12] A. Ferrario, N. Rucker, S. Wong, M. Luna, C.J. Gomer, Survivin, a member of the inhibitor of apoptosis family, is induced by photodynamic therapy and is a target for improving treatment response, Cancer Res. 67 (2007) 4989–4995, https://doi.org/10.1158/0008-5472.CAN-06-4785.
[13] N. Ahmad, K. Kalka, H. Mukhtar, *In vitro* and *in vivo* inhibition of epidermal growth factor receptor-tyrosine kinase pathway by photodynamic therapy, Oncogene 20 (2001) 2314–2317, https://doi.org/10.1038/sj.onc.1204313.
[14] T. Hama, Y. Yuza, Y. Saito, J. O-uchi, S. Kondo, M. Okabe, H. Yamada, T. Kato, H. Moriyama, S. Kurihara, M. Urashima, Prognostic significance of epidermal growth factor receptor phosphorylation and mutation in head and neck squamous cell carcinoma, Oncologist 14 (2009) 900–908, https://doi.org/10.1634/theoncologist.2009-0058.
[15] S. Wheeler, D.R. Siwak, R. Chai, C. LaValle, R.R. Seethala, L. Wang, K. Cieply, C. Sherer, C. Joy, G.B. Mills, A. Argiris, J.M. Siegfried, J.R. Grandis, A.M. Egloff, Tumor epidermal growth factor receptor and EGFR PY1068 are independent prognostic indicators for head and neck squamous cell carcinoma, Clin. Cancer Res. 18 (2012) 2278–2289, https://doi.org/10.1158/1078-0432.CCR-11-1593.
[16] K.K. Ang, B.A. Berkey, X. Tu, H.-Z. Zhang, R. Katz, E.H. Hammond, K.K. Fu, L. Milas, Impact of epidermal growth factor receptor expression on survival and pattern of relapse in patients with advanced head and neck carcinoma, Cancer Res. 62 (2002) 7350–7356 http://www.ncbi.nlm.nih.gov/pubmed/12499279.
[17] D.J. Chen, C.S. Nirodi, The epidermal growth factor receptor: a role in repair of radiation-induced DNA damage, Clin. Cancer Res. 13 (2007) 6555–6560, https://doi.org/10.1158/1078-0432.CCR-07-1610.
[18] S.R. Wedge, D.J. Ogilvie, M. Dukes, J. Kendrew, R. Chester, J.A. Jackson, S.J. Boffey, P.J. Valentine, J.O. Curwen, H.L. Musgrove, G.A. Graham, G.D. Hughes, A.P. Thomas, E.S.E. Stokes, B. Curry, G.H.P. Richmond, P.F. Wadsworth, A.L. Bigley, L.F. Hennequin, ZD6474 inhibits vascular endothelial growth factor signaling, angiogenesis, and tumor growth following oral administration, Cancer Res. 62 (2002) 4645–4655 http://www.ncbi.nlm.nih.gov/pubmed/12183421.
[19] F. Ciardiello, R. Caputo, V. Damiano, R. Caputo, T. Troiani, D. Vitagliano, F. Carlomagno, B.M. Veneziani, G. Fontanini, A.R. Bianco, G. Tortora, Antitumor effects of ZD6474, a small molecule vascular endothelial growth factor receptor tyrosine kinase inhibitor, with additional activity against epidermal growth factor receptor tyrosine kinase, Clin. Cancer Res. 9 (2003) 1546–1556 http://www.ncbi.nlm.nih.gov/pubmed/12684431.
[20] J. Schindelin, I. Arganda-Carreras, E. Frise, V. Kaynig, M. Longair, T. Pietzsch, S. Preibisch, C. Rueden, S. Saalfeld, B. Schmid, J.-Y. Tinevez, D.J. White, V. Hartenstein, K. Eliceiri, P. Tomancak, A. Cardona, Fiji: an open-source platform for biological-image analysis, Nat. Methods 9 (2012) 676–682, https://doi.org/10.1038/nmeth.2019.
[21] Q. Li, X. Wang, P. Wang, K. Zhang, H. Wang, X. Feng, Q. Liu, Efficacy of chlorin e6-mediated sono-photodynamic therapy on 4T1 cells, Cancer Biother. Radiopharm. 29 (2014) 42–52, https://doi.org/10.1089/cbr.2013.1526.
[22] W. Luo, R.-S. Liu, J.-G. Zhu, Y.-C. Li, H.-C. Liu, Subcellular location and photodynamic therapeutic effect of chlorin e6 in the human tongue squamous cell cancer Tca8113 cell line, Oncol. Lett. 9 (2015) 551–556, https://doi.org/10.3892/ol.2014.2720.
[23] H. Wang, L. Li, P. Wang, X. Wang, K. Zhang, Q. Liu, Comparison of photodynamic treatment produced cell damage between human breast cancer cell MCF-7 and its multidrug resistance cell, Photodiagnosis Photodyn. Ther. 16 (2016) 1–8, https://doi.org/10.1016/j.pdpdt.2016.07.004.
[24] C.E. Grossman, S.L. Carter, J. Czupryna, L. Wang, M.E. Putt, T.M. Busch, Fluence rate differences in photodynamic therapy efficacy and activation of epidermal growth factor receptor after treatment of the tumor-involved murine thoracic cavity, Int. J. Mol. Sci. 17 (11) (2016) E101, https://doi.org/10.3390/ijms17010101.
[25] S. Yazici, S.J. Kim, J.E. Busby, J. He, P. Thaker, K. Yokoi, D. Fan, I.J. Fidler, Dual inhibition of the epidermal growth factor and vascular endothelial growth factor phosphorylation for antivascular therapy of human prostate cancer in the prostate of nude mice, Prostate 65 (2005) 203–215, https://doi.org/10.1002/pros.20283.
[26] H.-Y. Tan, N. Wang, W. Lam, W. Guo, Y. Feng, Y.-C. Cheng, Targeting tumour microenvironment by tyrosine kinase inhibitor, Mol. Cancer 17 (2018) 43, https://doi.org/10.1186/s12943-018-0800-6.
[27] Q. Peng, Z. Deng, H. Pan, L. Gu, O. Liu, Z. Tang, Mitogen-activated protein kinase signaling pathway in oral cancer, Oncol. Lett. 15 (2018) 1379–1388, https://doi.org/10.3892/ol.2017.7491.
[28] K. Mishima, E. Yamada, K. Masui, T. Shimokawara, K. Takayama, M. Sugimura, K. Ichijima, Overexpression of the ERK/MAP kinases in oral squamous cell carcinoma, Mod. Pathol. 11 (1998) 886–891 http://www.ncbi.nlm.nih.gov/pubmed/9758369.
[29] L. Wang, T. Liu, M. Nishioka, R.L. Aguirre, S.S. Win, N. Okada, Activation of ERK1/2 and cyclin D1 expression in oral tongue squamous cell carcinomas: relationship between clinicopathological appearances and cell proliferation, Oral Oncol. 42 (2006) 625–631, https://doi.org/10.1016/j.oraloncology.2005.11.002.